# Resonant inelastic soft x-ray scattering, x-ray absorption spectroscopy, and density functional theory calculations of the electronic bulk band structure of CdS

L. Weinhardt,* O. Fuchs, and E. Umbach
*Experimentelle Physik II, Universität Würzburg, 97074 Würzburg, Germany*

C. Heske†
*Department of Chemistry, University of Nevada, Las Vegas, Nevada 89154-4003, USA*

A. Fleszar and W. Hanke
*Theoretische Physik I, Universität Würzburg, 97074 Würzburg, Germany*

J. D. Denlinger
*Advanced Light Source, Lawrence Berkeley National Laboratory, Berkeley, California 94720, USA*
(Received 8 September 2006; revised manuscript received 10 January 2007; published 30 April 2007)

The electronic bulk band structure of CdS was studied by resonant inelastic soft x-ray scattering and x-ray absorption spectroscopy. The measurements at the S *L*-edge are compared with theoretical spectra calculated with the Kramers-Heisenberg formalism and density functional theory. The experimental spectra reveal differences in the hole lifetimes of the different involved valence states, which can be correlated to different Auger decay probabilities. We find that the spectra are dominated by incoherent emission. However, a detailed comparison between measured and calculated spectra gives band structure information and, in particular, reveals the position of the valence band maximum within the emission spectra. Furthermore, the dephasing time in the intermediate state can be estimated.

DOI: 10.1103/PhysRevB.75.165207 PACS number(s): 71.20.Nr, 78.70.Ck, 71.15.Mb, 78.70.En

## I. INTRODUCTION

In recent years resonant inelastic x-ray scattering (RIXS) has been successfully developed as a technique for investigating the band structure of solids.[1] This technique exhibits several advantages and differences compared to the established photoelectron spectroscopy. As a "photon-in-photon-out" technique it is bulk sensitive and also allows the investigation of insulating samples. For RIXS with soft x-rays, the momentum of the photon can usually be neglected; in our case it is less than 10% of the width of the Brillouin zone of CdS. The *k* selectivity is then determined by the excitation energy independent on the sample orientation. Thus also polycrystalline and disordered samples such as powders can be studied. Furthermore, in some cases, the dipole selection rules allow to separate the emission from bands with different symmetry characters by choosing core levels with different angular momentum quantum numbers.[2] Finally, the intensity distribution gives quantitative information about the local distribution of the valence wave function with respect to the chosen core level wave function.

Several of the aspects mentioned above make the S $L_{2,3}$ emission of CdS very interesting. Since this emission probes valence states with *s* and *d* character, emission from Cd 4*d*-derived states, caused by an overlap with the S 2*p* core hole wave function can be observed. This was used with nonresonantly excited x-ray emission spectroscopy (XES) as a sensitive probe for the evidence of S-Cd bonds in several investigations. For instance, the chemical properties of buried interfaces, e.g., in CdS/ZnSe superlattices,[3] which are used for light-emitting diodes,[4] or $Cu(In,Ga)(S,Se)_2$ thin film solar cells[5–7] were investigated, taking advantage of the information depth of a few hundred nm. In addition to these applications, CdS is also used as nanoparticle material.[8,9] Such CdS nanoparticles were investigated with XES by Lüning *et al.*, who found size-dependent changes of the emission and absorption spectra and empirically extracted information about the increase in band gap caused by a local confinement.[10]

Apart from the chemical information from XES spectra, the electronic structure is of special importance for all mentioned applications. Therefore, several band structure calculations for CdS can be found in literature both for cubic CdS (Refs. 11–14) and wurtzite CdS.[15–17] There are also some very early experimental investigations of the CdS band structure using photoelectron spectroscopy.[18–21] However, a prerequisite for photoemission investigations is a well- prepared single crystalline sample surface, which is not present in the above-mentioned applications. Here, RIXS is an ideally suited technique. For CdS, there is only one early paper by Zhou *et al.*[22] reporting resonantly excited $L_{2,3}$ emission spectra of CdS. In that paper they also probed for resonant emission in their spectra but could not observe any.

Our measurements show that resonant effects are indeed small, but that, together with theoretical calculations, the resonant spectra give valuable information about the electronic structure of CdS. Furthermore, we will show how the measurements help to quantify different times cales involved in RIXS, namely the lifetime of valence holes in the final state and the dephasing time in the intermediate state.

## II. EXPERIMENT AND THEORY

The RIXS and near edge x-ray absorption fine structure (NEXAFS) spectra were recorded at the SXF endstation of

 

beamline 8.0 at the Advanced Light Source, Lawrence Berkeley Laboratory[23] using a CdS(0001) single crystal (Mateck, Jülich, Germany) with wurtzite structure. The experimental resolution of spectrometer and beamline were each chosen to be better than 0.3 eV. The NEXAFS spectra were recorded in the partial photon yield mode, i.e., the integral countrate of the S $L_{2,3}$ emission spectrum was taken as intensity. The NEXAFS acceptance window (ca. 146–160 eV) was chosen such that the elastic scattered peak (the Rayleigh line) was always outside the acceptance window. By measuring the Rayleigh line at various energies within the energy window of the emission spectrometer, RIXS- and NEXAFS-spectra were calibrated on a common energy scale.

The RIXS spectra for CdS were calculated on the bases of the Kramers-Heisenberg formalism and density functional theory,[24,25] which we have used successfully to describe RIXS spectra of BeSe and BeTe.[26] The local-density approximation[24,25] has been used together with $Cd^{20+}$ and $S^{14+}$ pseudopotentials generated according to the Hamann's method.[27] The binding energy of the semicore-*d* states is always underestimated in the local density approximation (LDA), therefore, in order to facilitate a comparison with the experimental spectra, the *d*-channel part of the bare Cd pseudopotential was adjusted in such a way that the Cd-4*d* states were moved to their experimentally observed position. This type of pseudopotential adjustment was similar to earlier calculations of the loss spectra of Cd-chalcogenides.[28,29] It should be noted, however, that the *bare* Cd-pseudopotential was adjusted, which thus affects the whole electronic structure of CdS via self-consistency. In particular, this has an effect on the valence-bandwidth, as will be discussed below. In addition, the energy position of the sulfur 2*p* states, in particular their spin-orbit splitting has been empirically adjusted to experiment. Unlike the Cd-4*d* states, however, this was done after the self-consistent solution had been obtained. When calculating the resonant spectra, the momentum of the photon has been neglected.

Valence-hole lifetimes due to electron-electron interactions were obtained within the GW approximation. The GW calculations were performed for the zinc-blende structure of CdS.[30] The lifetime broadening of the valence states was calculated for a uniform mesh of 32 $\vec{k}$-points within the zinc-blende Brillouin zone and the results were fitted to a quadratic function of the binding energy. The underlying assumption of this procedure is a similarity of the lifetime broadening between the wurtzite and the zinc-blende crystal structures.

## III. RESULTS AND DISCUSSION

### A. The incoherent S $L_{2,3}$ emission spectrum as derived by theory and experiment; valence hole lifetimes

The S $L_{2,3}$ XES spectrum of CdS with an excitation energy of 200 eV is shown in Fig. 1(a). It consists of three main features: Transitions from S 3*s*-derived states around 147.6 eV, from Cd 4*d*-derived states (150.6 eV and 151.8 eV), which have a large overlap with the S 2*p* core hole wave function, and from the upper valence band (UVB),

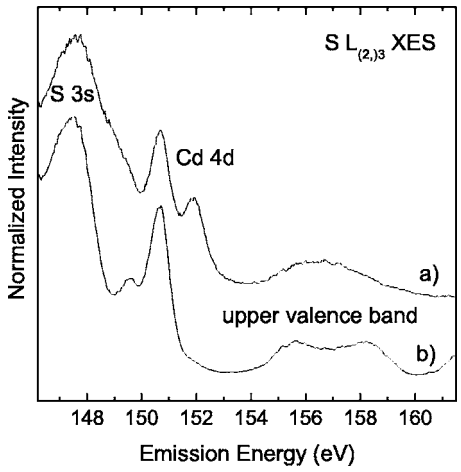


FIG. 1. (a) S $L_{2,3}$ emission spectrum excited with an excitation energy of 200 eV, (b) S $L_3$ emission spectrum of CdS excited with an excitation energy below the S $L_2$ absorption edge (162.0 eV $< h\nu_{exc} <$ 162.7 eV).

into S 2*p* core holes.[7,22,31] Each of these transitions forms a doublet because of the spin-orbit splitting of the S 2*p* core hole, which is clearly visible in the sharp transitions of the Cd 4*d*-like states. Neglecting the splitting and dispersion of the Cd 4*d*-derived states and thus the possible difference in line shape between transitions into S $2p_{1/2}$ and S $2p_{3/2}$ core holes, we simply derive the spin-orbit splitting from the distance of the two lines and get a value of 1.2 eV, which is in good agreement with the values found in literature.[3,22,32,33]

By choosing a suitable excitation energy, a distinction between the features from transitions into S $2p_{1/2}$ and S $2p_{3/2}$ holes can be made. For doing so, we have chosen excitation energies just below the S $L_2$ absorption edge. Since the spin-orbit splitting between the two S 2*p* levels is only 1.2 eV, the excitation energy is close to the S $L_3$ absorption edge and resonant effects are expected. However the spectral changes with excitation energy are only small, as will be discussed below. To obtain better statistics, we have thus added up eight spectra with different excitation energies from 162.0 eV to 162.7 eV, and will, in a first step, treat the resulting sum spectrum shown in Fig. 1(b) as "incoherent" (i.e., a spectrum devoid of resonant effects).

In Fig. 2, the $L_3$ spectrum is now compared with the calculated band structure, the corresponding total density of states (DOS), and the local partial density of states (LPDOS). For doing so, the emission energy scale of the experimental spectrum was adjusted to the binding energies relative to the valence band maximum (VBM; the determination of its position within the experimental spectra is discussed below). The emission energy of the VBM at 159.4 eV corresponds to the binding energy of the S $2p_{3/2}$ core level with respect to the VBM and will be used for all further comparisons between theory and experiment. The DOS shown in Fig. 2 underlines the assignment of the different spectral features given above. In fact, the calculated position of the 3*s* levels at about 12 eV agrees very well with the observed spectrum. The Cd 4*d*-derived levels between 8 and 10 eV split into 20 states for CdS in the wurtzite structure (two Cd atoms per unit cell) and show a dispersion of about 1 eV. The DOS of

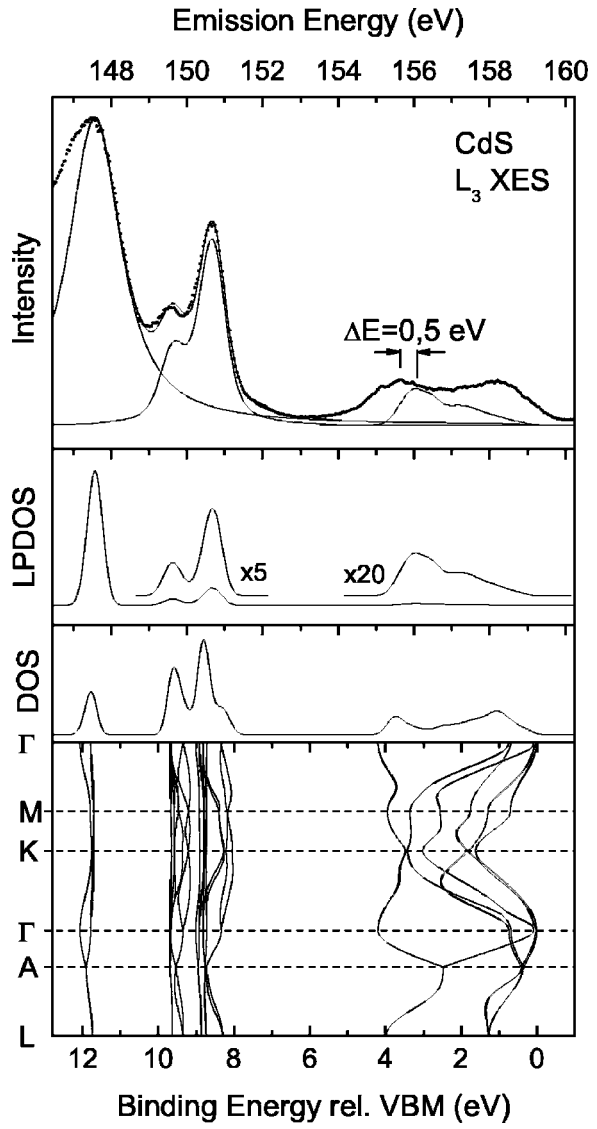


FIG. 2. Comparison of the S $L_3$ emission spectrum (top, dots) of CdS with the calculated band structure, the total density of states as well as the LPDOS. The experimental $L_3$ emission spectrum is shown together with the broadened LPDOS. For details see text.

the *d*-bands has two distinct maxima and a shoulder, which are qualitatively in good agreement with the observed features in the $L_3$ emission spectrum. For a quantitative comparison with the experimental spectrum, the LPDOS was calculated by taking the dipole matrix element of the emission process into account,

$$\mathrm{LPDOS}(E) = \sum_{i,f} \int |\langle \psi_{f,\vec{k}} | \hat{p} | \psi_{i,\vec{k}} \rangle|^2 \delta[E - E_i(\vec{k}) + E_f(\vec{k})] d^3k, \tag{1}$$

where $\psi_{i,\vec{k}}$ and $\psi_{f,\vec{k}}$ are the initial (valence) states and final states (here S $2p$), respectively. The LPDOS calculated in this way is shown in Fig. 2. It can be understood as an incoherent spectrum after including the experimental broadening of the spectrometer of 0.3 eV.

In order to also include the lifetime broadening, the calculated emission from S $3s$-derived states and Cd $4d$-derived states was convoluted with suitable Lorentzian functions. Different Lorentzian widths were used for S $3s$- and Cd $4d$-derived states, respectively, and adjusted for an optimal description of the experimental spectrum. For the S $3s$-derived states this adjustment was done at the high energy side of the corresponding emission. The result of this procedure is shown in Fig. 2 together with the experimental spectrum. In general, good agreement between theory and experiment is achieved. The only significant deviation is found on the side of lower emission energy of the S $3s$ peak and was previously ascribed by Zhou *et al.* to inelastic losses.[22]

The LPDOS much better describes the ratio between the emission from S $3s$- and Cd $4d$-derived states than the DOS. It demonstrates that the wave function of the Cd $4d$-derived states is more localized at the Cd atoms and the overlap with the S $2p$ wave function is lower than that of the S $3s$-derived states, as expected. However, for optimal agreement between theory and experiment (topmost spectrum in Fig. 2) the calculated emission from the Cd $4d$-derived states had to be multiplied with respect to the S $3s$ emission by a (relatively small) factor of 1.5. Furthermore, we have also magnified the UVB by a factor of 1.6 for better comparison. The reason for these factors is probably an underestimation of the corresponding matrix elements by the calculations. Moreover, the additional (nonsymmetric) intensity at the low-energy side of the S $3s$ peak due to the above-mentioned inelastic losses could also contribute.

We note that the peak area of the theoretical UVB structure is approximately one-half of that in the experimental spectrum (after the above-mentioned scaling). This could be due to a variety of origins: First, we note that the spectrum is taken 1 eV above the threshold, and hence has a contribution of resonant character. Second, excitonic effects (which are strong in this system and will be discussed in detail below) could lead to a different average over *k*-space and hence a modified matrix element as compared to the theoretical (nonresonant) case. Finally, the relative weight of *s* vs *p* character in the valence band (as a function of position in the Brillouin zone) might not be optimally described by theory.

As a result of the above linewidth optimization, we can derive lifetime broadenings for the emission from the S $3s$-derived states of 1.5 eV and for the Cd $4d$-derived states of 0.4 eV. These lifetime broadenings include the lifetime of the S $2p_{3/2}$ core hole and that of the respective valence hole. The S $2p_{3/2}$ lifetime is equal for both transitions and can be neglected since it is around 50–60 meV.[34,35] The much larger lifetime broadening of the emission from the S $3s$ states compared to the Cd $4d$ states must thus be attributed to a much shorter lifetime of the hole in the S $3s$ states and can be explained as follows. The dominating electronic decay process for the investigated valence holes are Auger processes. In order to emit an Auger electron, there must be enough energy gain by filling the initial hole with another electron. Neglecting the involved matrix elements, it is apparent, that this can be much more easily achieved for the deeper-lying S $3s$ derived states, explaining their shorter lifetime. This qualitative consideration can be quantitatively confirmed by theoretical calculations. For that purpose, we

TABLE I. Experimental and theoretical values for the width of the UVB of wurtzite CdS from this work and other papers.

| Method | Valence-band width | Reference |
|---|---|---|
| X-ray emission | 4.6 eV | This work |
| Angle resolved photoelectron Spectroscopy | 4.5 eV | 19 |
| Monochromatized Al $K_\alpha$ Photoelectron spectroscopy | 4.8 eV | 18 |
| LDA with shifted Cd-4*d* states | 4.10 eV | This work |
| Standard LDA | 4.52 eV | This work |
| Standard LDA | 4.20 eV | 15 |
| Standard LDA | 4.32 eV | 16 |
| LDA with SIC-PP | 4.50 eV | 16 |
| LDA with SIRC-PP | 4.60 eV | 17 |

have calculated the lifetime broadening caused by Auger decays for 32 different $k$ vectors and then extrapolated onto the whole $k$ space. As a result, we get values of 0.9 eV for the S 3*s* states and 0.10 eV for the Cd 4*d* states, showing the same tendency as observed in the measurements. However, both values are smaller than those derived from the measurements. A reason for that could be an additional broadening due to phonons not included in the calculations or a possible underestimation of the theoretical bandwidth of the S 3*s*- and Cd 4*d*-derived states, leading to artificially high values for the experimental lifetime broadening derived by our convolution approach.

The agreement between the theoretical spectrum of the upper valence band and the experimental spectrum is not as good as in the case of the S 3*s*- and Cd 4*d*-derived states. In Fig. 2 the calculated spectrum of the UVB is shown (including the experimental broadening of 0.3 eV) in comparison with the experimental spectrum. It can clearly be seen that the maximum close to the VBM in the experimental spectrum cannot be reproduced by the calculated incoherent spectrum. As mentioned above, this can be explained by taking the coherent fraction of the spectrum into account, which will be done in Sec. III C. Another discrepancy between theory and experiment is that the UVB emission in the experiment extends to lower photon energies than in the theoretical spectrum. This is quantified in Fig. 2 by evaluating the shift between the maxima at the low photon energy side of the UVB emission, which is around 0.5 eV. Starting from a calculated bandwidth of 4.1 eV, we thus get a "modified experimental" value for the width of the UVB of 4.6 eV (note that the VBM of experiment and theory were aligned for all comparisons between experiment and theory, as mentioned above). This is in good agreement with other experimental values, as shown in Table I. In this table also theoretical values are summarized. It follows that the *p*-valence-band width of CdS is reduced by ca. 0.4 eV in our calculation when the Cd-4*d* states are constrained to have their experimental binding energy. We note, however, that our "standard" LDA calculation agrees well with other LDA results.

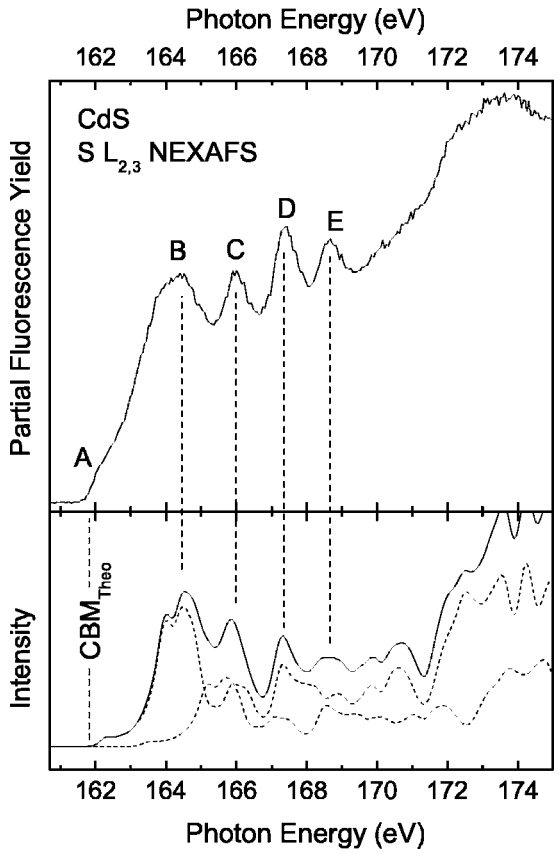


FIG. 3. Experimental (top) and calculated (bottom) S $L_{2,3}$ NEXAFS spectra of CdS. Below the calculated S $L_{2,3}$ spectrum, the S $L_2$ and $L_3$ contributions are shown separately (dashed lines). "$CBM_{Theo}$" denotes the conduction-band minimum in the calculations.

Altogether, it seems that the LDA calculations tend to slightly underestimate the true bandwidth of the UVBs. This has been discussed elsewhere.[36]

### B. The NEXAFS spectrum of CdS

In Fig. 3 the partial fluorescence NEXAFS spectrum of CdS is shown and compared with the calculated absorption spectrum. The calculated spectrum takes the density of states and the matrix elements into account, while excitonic effects due to the presence of the core hole are not included. The calculation is furthermore convoluted with a Gaussian of 0.3 eV width, corresponding to the experimental resolution of the beamline. The absorption onset is marked with *A*. In the literature, several different interpretations of this structure are discussed. Sugiura *et al.* and Zhou *et al.* identify it with the conduction-band minimum (CBM),[22,37] whereas in a more recent paper by Lüning *et al.* it is identified with the excitation of a core exciton.[10] The latter assignment is based on a measurement series with CdS nanoparticles of different sizes, where feature *A* increasingly separates from the rest of the spectrum for smaller particles. This is explained by an increase in binding energy of the core exciton due to an increase in the spatial confinement.[10]

The comparison between experiment and theory, however, shows that both interpretations are only partially true. We find an excellent agreement in peak position (see features *B* through *E*) between theory and experiment in the region between 165 and 169 eV. Note that both the theoretical and experimental absorption spectra are on a common energy scale with the emission spectra and therefore the same relative adjustment of the energy scale as for the emission spectra was used. In the region of the absorption edge, we find that the energetic position of the edge can easily be associated with the conduction-band minimum. However, just above the onset the experimental spectrum has a significantly higher intensity than the calculated one. This can be attributed to excitations into a core exciton state, which is not included in the calculation. The fact that this potential core excitation takes place *above* the CBM indicates that observable excitations do not occur below the CBM at the Γ-point, but take place at other energetically higher states with vanishing group velocities (i.e., higher states at the Γ-point or excitations at other high symmetry points).

As a result of the above procedure, it is possible to determine the position of the CBM on the "photon energy" scale. Together with the detailed analysis of the RIXS spectra we can derive the electronic band gap of the material. In our case, we have used the literature band gap of 2.47 eV (Ref. 38) to align the theoretical spectra, finding a very good agreement for the position of the NEXAFS maxima as described above.

### C. The S $L_{2,3}$ RIXS spectra

In this section resonant effects found close to the absorption threshold are discussed. For that purpose, a series of S $L_{2,3}$ spectra with excitation energies from below the S $L_3$ absorption edge up to about 1.5 eV above the $L_2$ absorption edge were recorded.

In Fig. 4 a series of resonant S $L_{2,3}$ emission spectra are shown. The excitation energy is given on the right-hand side of the graph. With decreasing excitation energy, less S $2p_{1/2}$ core holes are created and therefore the $L_2$ emission (as seen, e.g., by the peak at 151.9 eV) decreases until it is fully absent at an excitation energy of 162.9 eV. Close to the emission from the VBM, a shift of the feature labeled $A_2$ can be observed. This can be attributed to coherent S $L_2$ emission shifting towards the VBM when the excitation approaches the CBM. A quantitative evaluation of this effect for the S $L_2$ emission is difficult since it is superimposed with the S $L_3$ emission. Note that the increasing background above an emission energy of ca. 160.5 eV is due to the elastically scattered Rayleigh line.

For the S $L_3$ emission such a superposition does not occur for energies below the S $L_2$ threshold, which makes a quantitative evaluation of the coherent part in the spectrum possible. The spectra are composed of incoherent emission, dominating the spectra as discussed in Sec. III A, and a coherent part. Furthermore, the NEXAFS spectrum presented above shows that emission with a core exciton in the intermediate state must be taken into account. The influence of such excitonic intermediate states has been treated in several

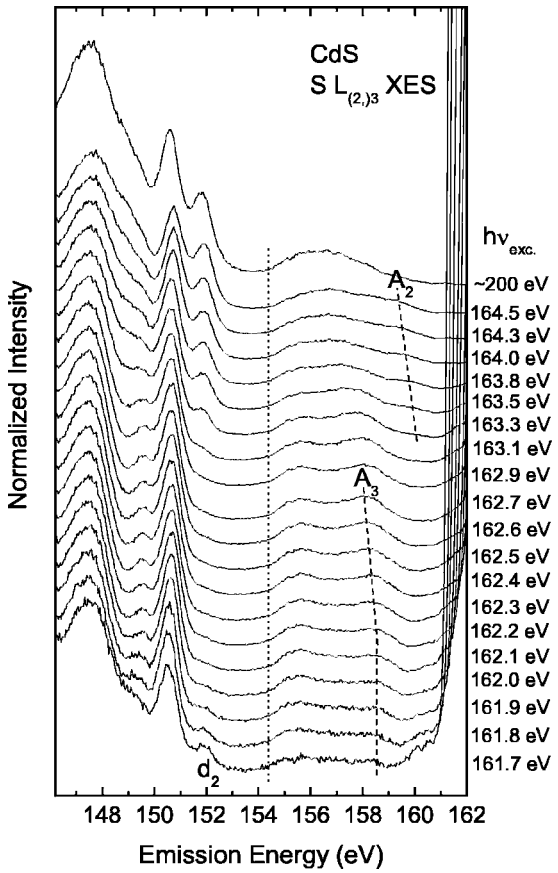


FIG. 4. Resonant and one nonresonant S $L_{2,3}$ emission spectra of CdS. The excitation energies are given on the right-hand side. All spectra were normalized to their maximum at approximately 147.5 eV. Only the nonresonant spectrum has been multiplied by 1.5 to enlarge the upper valence-band emission. The high intensity above 160.5 eV is due to the Rayleigh line moving into the window with decreasing excitation energy.

experimental and theoretical papers (e.g., Refs. 39–43). In most cases the influence of the core exciton is smaller in the emission spectra than in the absorption spectra since the core exciton is only present in the intermediate state.

In general, three different core exciton effects are reported. The first is the participant decay, which is caused by a localization of the exciton in the intermediate state. This strongly enhances a direct recombination of electron and hole (i.e., the elastic scattered peak). Indeed, such an increase can be found in our experiments (see the overlapping sharp lines above 161 eV). The second effect can be observed at the so-called "second threshold."[44] Again, the excited electron directly recombines with the core hole, but in addition the energy is sufficient to excite an electron from the valence band into the conduction band. Such effects were for example found for BeTe and BeSe (Ref. 26) but were not investigated in this work. The third effect is the spectator decay. In contrast to the participant decay, in this case an electron from the valence band recombines with the core hole. Since the core exciton is thereby transformed to a valence exciton with lower binding energy, the emission shifts to lower emission energies. This should be visible as additional intensity below the low energy side of the UVB emis-

sion. However, in our spectra, no such additional intensity can be found: in Fig. 4 the dotted line at 154.5 eV is a reasonable lower bound for all resonant spectra as well as for the spectrum taken at high excitation energy, which is free of excitonic effects. In accordance with experimental and theoretical results of Carlisle *et al.* and Shirley[42,43] for graphite, we do not find any changes in the spectral shape caused by core-excitonic intermediate states. In fact, the excitonic excitations only change the overall intensity of the spectra, as argued by Carlisle *et al.*[43] In this scenario the final states are reached by scattering with phonons, whereby the emission cannot be distinguished from incoherent emission without a core exciton in the intermediate state.

As discussed above, most of the $L_3$ spectra can be described by the calculated incoherent spectrum, which is independent of the excitation energy. The spectral changes occurring below $h\nu$=162.0 eV, most prominently the feature marked with $d_2$, are due to a reemerging of the $L_2$ emission. This emission is caused by multiples of the nominal excitation photon energy stemming from higher harmonics of the undulator with corresponding higher orders of the monochromator and gains in weight at the absorption threshold due to the reduced "true" emission intensity which is also observed as enhanced noise in the normalized spectra. Upon closer inspection, however, a resonant feature can be found, labeled $A_3$ in Fig. 4. Similar to $A_2$, it shifts to higher emission energies with decreasing excitation energy. Below an excitation energy of 162.2 eV, the position is nearly constant, and $A_3$ decreases in relative intensity (again, the feature emerging at emission energies above 159 eV is the onset of the elastically scattered peak).

The *coherent* contributions to the spectra have been calculated using the Kramers-Heisenberg formalism and are shown in Fig. 5. The emission from S 3*s*- and Cd 4*d*-derived states are convoluted with the lifetime broadening derived above, while the emission from the UVB was not additionally broadened (note that this artificially enhances the peak height of the valence-band peak compared to the 3*s* emission). The calculated emission from the S 3*s*-derived states does not show any dependence on the excitation energy because their dispersion is small and, in addition, they have a large lifetime broadening. The spectral changes of the emission from the Cd 4*d*-derived states are also small, explaining why they cannot be observed in the experimental spectra, which are dominated by noncoherent emission.

The strongest changes can be found in the UVB, as expected. To understand their origin, a cutout of the calculated band structure is shown in the inset of Fig. 5. Two dispersing features are found in the spectra, which are labeled "1" and "2" and also marked in the band structure. For the lowest excitation energies, excitation and emission take place at the Γ-point. However, the matrix element of emission from the VBM is very small due to its predominantly *p*-like symmetry character, so that the peak labeled "1" stems from states about 1 eV below the VBM with an appreciable *s*-like character. With increasing excitation energy, excitation and emission move away from the Γ-point towards higher $k$ values (see arrows in the inset of Fig. 5). As indicated in the band structure, this leads to a shift of peak 1 towards lower emission energies, which is in good agreement with the shift of

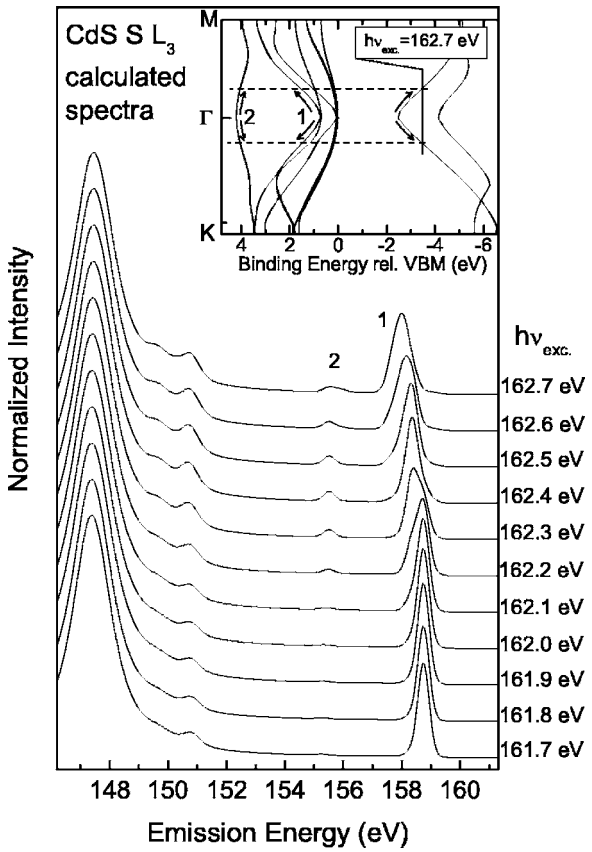


FIG. 5. Calculated coherent $L_3$ emission spectra of CdS. The corresponding excitation energies are given on the right-hand side. The inset shows a cutout of the calculated band structure.

peaks $A_3$ and $A_2$ in Fig. 4. In parallel, peak 2 shifts towards higher emission energies, but since the intensity of this feature is very small and overlaps with the incoherent valence-band emission, it cannot be found in the experimental spectra.

For a better quantification it is desirable to extract the coherent part of the experimental spectra. The standard method (see, e.g., Refs. 1 and 2) is to take a spectrum excited high above the absorption threshold as an approximation of the incoherent spectrum and to subtract it, multiplied by a suitable weight factor, from the resonantly excited spectra. However, this method cannot easily be used in the present case, since, for excitation energies high above the absorption threshold, the contribution of $L_2$ and $L_3$ emission cannot be experimentally separated. Lüning *et al.* solved this problem for Si $L_{2,3}$ by assuming an intensity ratio of 2 and a fixed spin-orbit splitting between $L_3$ and $L_2$ emission, and by extracting the $L_3$ part from the spectrum excited high above the absorption threshold.[2] Since, in our case, the coherent part is very small, we have developed a different approach. We have subtracted the spectrum taken with an excitation energy of 162.7 eV, i.e., the highest-excited spectrum below the $L_2$ absorption threshold, from the other resonant $L_3$ spectra (all spectra were normalized to their maximum). By doing so, all parts of the spectra which do not show an excitation energy dependence (i.e., the incoherent part), should be eliminated. The remaining features now represent the changes of the

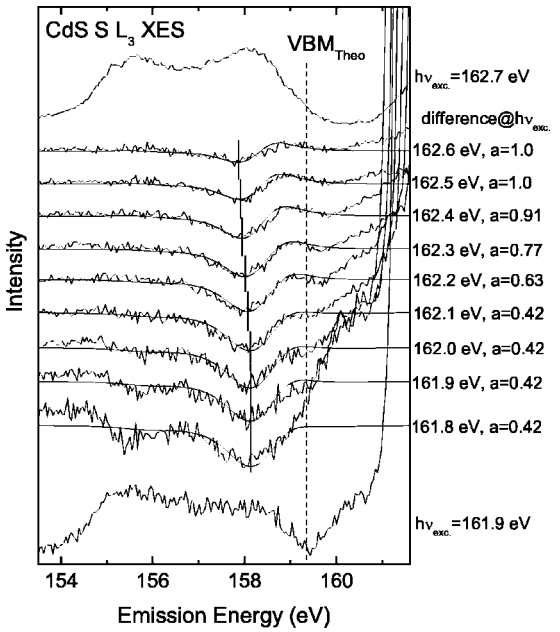


FIG. 6. $L_3$ emission spectra of the upper valence band for two different excitation energy (top-most and bottom-most spectrum). In between, experimental and theoretical difference spectra are given for different excitation energies (see text). For the theoretical differences an additional parameter $a$ is used (see text). The dashed line marks the position of the VBM in the theoretical spectra.

coherent part, and can be compared with differences of the theoretical spectra constructed in an analogous way.

The differences of the experimental and theoretical spectra are shown in Fig. 6. For the experimental differences, the normalized spectra were directly subtracted from each other. In contrast, the theoretical difference $D_T$ for an excitation energy of $h\nu_{\mathrm{exc}}$ was calculated as follows:

$$D_T = S(a \text{ spectrum } @\ h\nu_{\mathrm{exc}} - \text{spectrum } @\ 162.7 \text{ eV}). \tag{2}$$

The factor $S$ is introduced because the theoretical spectrum only includes coherent emission, while a part of the experimental spectrum is due to incoherent emission. Because this incoherent part dominates the experimental spectrum it is approximately canceled out in the subtraction process and therefore $S$ describes the ratio between the coherent part and the incoherent part in the experimental spectra. The additional factor $a$ takes the excitation energy dependence of this ratio into account. Finally, the theoretical spectra were convoluted with a Lorentzian with a width of 1.0 eV. Since electron-electron interactions are expected to be weak for the considered energies, the lifetime broadening can presumably be attributed to electron-phonon scattering. $S$, which was kept constant at 0.28 for all excitation energies, and $a$ were optimized to give best agreement between the experimental and theoretical difference curves (shown in Fig. 6). As can be seen in Fig. 6, the agreement between theory and experiment is excellent (see also the short vertical lines that indicate the minimum in the theoretical difference curves). The theoretical position of the VBM shown in Fig. 6 can therefore be assumed to be also the position of the VBM within the experimental spectra. The coherent fraction of the spectra can be related to the dephasing process in the intermediate state. However, an exact evaluation is difficult, because—apart from the incoherent fraction caused by dephasing processes—the excitonic excitations lead to additional incoherent emission. Therefore, only a lower limit for the dephasing time can be given. For doing so, the coherent fraction in the spectrum excited with 162.7 eV was estimated using the scaling factor $S$. $S$ must be modified by a correction factor taking into account that $S$ was derived from spectra normalized to their maximum count rate (see above), while the true coherent fraction $f$ needs to be based on the overall integrated intensities of the experimental and theoretical spectra, respectively. Applying this correction, we derive $f=0.26$ for the spectrum excited at 162.7 eV. Using the "core hole clock" formalism[45] and the S $2p$ core hole lifetime $\tau_{ch}=\hbar/60$ meV$=11$ fs,[34] a lower limit for the dephasing time $\tau_d > \tau_{ch}/(1/f-1)$ can be calculated and we obtain 3.9 fs.

An interpretation of the parameter $a$ with respect to the energy dependence of the dephasing time fails because the part of the emission with excitonic intermediate state is unknown and expected to vary strongly with excitation energy.

## IV. SUMMARY

We have investigated the bulk electronic structure of CdS using resonant inelastic soft x-ray scattering and x-ray absorption. We find that the measured spectra are dominated by incoherent emission. For the emission from S $3s$- and Cd $4d$-derived states, an excellent agreement between experiment and calculated incoherent spectra is achieved. We find a significantly larger lifetime broadening for the S $3s$-derived states than for the Cd $4d$-derived states, which can be explained by different Auger decay probabilities of the holes in these states. With the excitation energy close to the $L_2$ and $L_3$ absorption thresholds, we find resonant effects in our spectra, which can be well described by calculations based on the Kramers-Heisenberg formalism. As a result, we determine the position of the VBM within the S $L_3$ emission spectrum, which is of fundamental importance for determining band gaps (e.g., of nanoparticles). Up to now much simpler approaches (i.e., linear extrapolation of the leading edge), not taking into account the actual electronic structure and resonant effects, had to be used.[10,22] Finally, we were able to extract information about the time scale of the dephasing processes in the intermediate state.

## ACKNOWLEDGMENTS

The authors gratefully acknowledge funding by the DFG through SFB 410, TP B3, TP B4, and TP A3. The Advanced Light Source is supported by the Director, Office of Science, Office of Basic Energy Sciences, Materials Sciences Division, of the U.S. Department of Energy under Contract No. DE-AC03-76SF00098 at Lawrence Berkeley National Laboratory. The calculations were performed at the ZAM Jülich.

*Electronic address: weinhard@unlv.nevada.edu; present address: Department of Chemistry, University of Nevada, Las Vegas, NV 89154-4003.
†Electronic address: heske@unlv.nevada.edu

[1] S. Eisebitt and W. Eberhardt, J. Electron Spectrosc. Relat. Phenom. **110–111**, 335 (2000).
[2] J. Lüning, J.-E. Rubensson, C. Ellmers, S. Eisebitt, and W. Eberhardt, Phys. Rev. B **56**, 13147 (1997).
[3] C. Heske, U. Groh, O. Fuchs, L. Weinhardt, E. Umbach, M. Grün, S. Petillon, A. Dinger, C. Klingshirn, W. Szuszkiewicz *et al.*, Appl. Phys. Lett. **83**, 2360 (2003).
[4] M. Schmidt, M. Grün, S. Petillon, E. Kurtz, and C. Klingshirn, Appl. Phys. Lett. **77**, 85 (2000).
[5] C. Heske, D. Eich, R. Fink, E. Umbach, T. van Buuren, C. Bostedt, L. Terminello, S. Kakar, M. Grush, T. Callcott *et al.*, Appl. Phys. Lett. **74**, 1451 (1999).
[6] C. Heske, D. Eich, R. Fink, E. Umbach, S. Kakar, T. van Buuren, C. Bostedt, L. Terminello, M. Grush, T. Callcott *et al.*, Appl. Phys. Lett. **75**, 2082 (1999).
[7] C. Heske, U. Groh, O. Fuchs, E. Umbach, N. Franco, C. Bostedt, L. Terminello, R. Perera, K. Hallmeier, A. Preobrajenski *et al.*, Phys. Status Solidi A **187**, 13 (2001).
[8] A. D. Dinsmore, D. S. Hsu, S. B. Qadri, J. O. Cross, T. A. Kennedy, H. F. Gray, and B. R. Ratna, J. Appl. Phys. **88**, 4985 (2000).
[9] M. Bruchez, M. Moronne, P. Gin, S. Weiss, and A. P. Alivisatos, Science **281**, 2013 (1998).
[10] J. Lüning, J. Rockenberger, S. Eisebitt, J.-E. Rubensson, A. Karl, A. Kornowski, H. Weller, and W. Eberhardt, Solid State Commun. **112**, 5 (1999).
[11] P. Rinke, A. Qteish, J. Neugebauer, C. Freysoldt, and M. Scheffler, New J. Phys. **7**, 126 (2005).
[12] M. Rohlfing, P. Krüger, and J. Pollmann, Phys. Rev. Lett. **75**, 3489 (1995).
[13] M.-Z. Huang and W. Y. Ching, Phys. Rev. B **47**, 9449 (1993).
[14] A. Zunger and A. J. Freeman, Phys. Rev. B **17**, 4850 (1978).
[15] P. Schröer, P. Krüger, and J. Pollmann, Phys. Rev. B **48**, 18264 (1993).
[16] D. Vogel, P. Krüger, and J. Pollmann, Phys. Rev. B **52**, R14316 (1995).
[17] D. Vogel, P. Krüger, and J. Pollmann, Phys. Rev. B **54**, 5495 (1996).
[18] L. Ley, R. A. Pollak, F. R. McFeely, S. P. Kowalczyk, and D. A. Shirley, Phys. Rev. B **9**, 600 (1974).
[19] N. G. Stoffel, Phys. Rev. B **28**, 3306 (1983).
[20] A. P. J. Stampfl, P. Hofmann, O. Schaff, and A. M. Bradshaw, Phys. Rev. B **55**, 9679 (1997).
[21] K. O. Magnusson and S. A. Flodström, Phys. Rev. B **38**, 1285 (1988).
[22] L. Zhou, T. A. Callcott, J. J. Jia, D. L. Ederer, and R. Perera, Phys. Rev. B **55**, 5051 (1997).
[23] J. J. Jia, T. A. Callcott, J. Yurkas, A. W. Ellis, F. J. Himpsel, M. G. Samant, J. Stöhr, D. L. Ederer, J. A. Carlisle, E. A. Hudson *et al.*, Rev. Sci. Instrum. **66**, 1394 (1995).
[24] P. Hohenberg and W. Kohn, Phys. Rev. **136**, B864 (1964).
[25] W. Kohn and L. J. Sham, Phys. Rev. **140**, A1133 (1965).
[26] D. Eich, O. Fuchs, U. Groh, L. Weinhardt, R. Fink, E. Umbach, C. Heske, A. Fleszar, W. Hanke, E. Gross *et al.*, Phys. Rev. B **73**, 115212 (2006).
[27] D. R. Hamann, Phys. Rev. B **40**, 2980 (1989).
[28] A. Fleszar and W. Hanke, Phys. Rev. B **56**, 12285 (1997).
[29] H. Dröge, A. Fleszar, W. Hanke, M. Sing, M. Knupfer, J. Fink, F. Goschenhofer, C. R. Becker, R. Kargerbauer, and H.-P. Steinrück, Phys. Rev. B **59**, 5544 (1999).
[30] A. Fleszar and W. Hanke, Phys. Rev. B **71**, 045207 (2005).
[31] A. Meisel, I. Steuer, and R. Szargan, Spectrochim. Acta, Part B **23**, 527 (1968).
[32] E. Gedat, R. Püttner, M. Domke, and G. Kaindl, J. Chem. Phys. **109**, 4471 (1998).
[33] M. Coville and T. D. Thomas, J. Electron Spectrosc. Relat. Phenom. **71**, 21 (1995).
[34] M. O. Krause and J. H. Oliver, J. Phys. Chem. Ref. Data **8**, 329 (1979).
[35] E. Kukk, J. D. Bozek, J. A. Sheehy, P. W. Langhoff, and N. Berrah, J. Phys. B **33**, L51 (2000).
[36] C. Heske, R. Treusch, F. J. Himpsel, S. Kakar, L. J. Terminello, H. J. Weyer, and E. L. Shirley, Phys. Rev. B **59**, 4680 (1999).
[37] C. Sugiura, Y. Hayasi, H. Konuma, and S. Kiyono, J. Phys. Soc. Jpn. **31**, 1784 (1971).
[38] K. J. Hong, T. S. Jeong, C. J. Yoon, and Y. J. Shin, J. Cryst. Growth **218**, 19 (2000).
[39] P. A. Brühwiler, P. Kuiper, O. Eriksson, R. Ahuja, and S. Svensson, Phys. Rev. Lett. **76**, 1761 (1996).
[40] J. A. Carlisle, E. L. Shirley, E. A. Hudson, L. J. Terminello, T. A. Callcott, J. J. Jia, D. L. Ederer, R. C. C. Perera, and F. J. Himpsel, Phys. Rev. Lett. **76**, 1762 (1996).
[41] M. van Veenendaal and P. Carra, Phys. Rev. Lett. **78**, 2839 (1997).
[42] E. L. Shirley, Phys. Rev. Lett. **80**, 794 (1998).
[43] J. A. Carlisle, E. L. Shirley, L. J. Terminello, J. J. Jia, T. A. Callcott, D. L. Ederer, R. C. C. Perera, and F. J. Himpsel, Phys. Rev. B **59**, 7433 (1999).
[44] W. L. O'Brien, J. Jia, Q.-Y. Dong, T. A. Callcott, K. E. Miyano, D. L. Ederer, D. R. Mueller, and C.-C. Kao, Phys. Rev. Lett. **70**, 238 (1993).
[45] O. Björneholm, A. Nilsson, A. Sandell, B. Hernnäs, and N. Mårtensson, Phys. Rev. Lett. **68**, 1892 (1992).